

New Evidence for Neutrino Flux Variability from Super-Kamiokande Data

D.O. Caldwell

Physics Department, University of California, Santa Barbara, CA 93106-9530, USA

P.A. Sturrock

Center for Space Science and Astrophysics, Stanford University, Stanford, CA 94305-4060, USA

(Dated: June 26, 2019)

While KamLAND apparently rules out Resonant-Spin-Flavor-Precession (RSFP) as an explanation of the solar neutrino deficit, the solar neutrino fluxes in the Cl and Ga experiments appear to vary with solar rotation. Added to this evidence, summarized here, a power spectrum analysis of the Super-Kamiokande (SK) data reveals variation in the flux matching a dominant rotation rate observed in the solar magnetic field in the same time period. A recent SK paper reporting no time variation of the flux did not take full account of the SK data, but instead focused on an alias frequency resulting from the very regular binning. RSFP or SFP may be a subdominant solar neutrino process occurring in the convection zone. The neutrino data show changes that correspond to solar-cycle changes in the magnetic field, typical of the convection zone. Analysis of SNO data when it becomes available will provide a valuable check on the current analysis of SK data and may make it possible to determine if neutrinos are Majorana particles. New physics appears needed to explain the solar neutrino flux variability, requiring not only a large neutrino transition magnetic moment, but also sterile neutrinos, if this is a subdominant process.

PACS numbers: 26.65.+t, 95.75.Wx, 14.60.St

INTRODUCTION

Recent results from the KamLAND experiment [1] seem to confirm the Large-Mixing Angle (LMA) solution to the solar neutrino deficit and rule out the Resonant-Spin-Flavor-Precession (RSFP) explanation [2]. On the other hand, there is increasing evidence [3]-[9] that the solar neutrino flux is not constant as assumed for the LMA solution, but varies with well-known solar rotation periods. The solar neutrino situation may be complex, and Spin-Flavor-Precession (SFP) [10] or RSFP could be subdominant to LMA, but either one appears to require at least one light sterile neutrino. Since this recent information on solar neutrino variability is not widely known, a brief summary is presented here of analyses of radiochemical neutrino data, along with new input from the Super-Kamiokande experiment [11]. While the 10-day averages of Super-Kamiokande solar neutrino data [12] show no obvious time dependence, power-spectrum analyses [13] displayed a strong peak at the frequency $26.57 \pm 0.05 \text{ y}^{-1}$ (period 13.75 d), as well as one at 9.42 y^{-1} . However, a subsequent Super-Kamiokande paper [14] provided 5-day averages of the data, and there was no longer evidence for the 26.57 y^{-1} peak, showing it to be an alias of the 9.42 y^{-1} peak (which will be explained later) due to the extremely regular 10-day binning. In the 5-day data the 9.42 y^{-1} frequency persists, and we also find a peak of the same frequency as a dominant oscillation (due to rotation) in the solar magnetic field.

If the KamLAND result is correct, a varying neutrino flux must be explained by a subdominant process. This could be SFP, in which the solar ν_e is changed by a transition magnetic moment to a different flavor, as in an

MSW process [15], but in addition its spin is flipped. The same type of transition occurs in RSFP, but in this case the mass difference between the neutrino states is such that RSFP is resonant in the Sun, just as for MSW. That the subdominant process is RSFP, rather than SFP, is suggested by some features of the flux data. For either process it appears necessary to have sterile neutrinos. For SFP the solution could be very similar to that of de Holanda and Smirnov [16], who suggested that adding a subdominant transition to a sterile neutrino would provide better agreement with both the Homestake data [17] and the Super-Kamiokande energy dependence [11], except that the sterile neutrino mixing would be replaced by magnetic moment transitions. In the RSFP case the two processes, MSW and RSFP, would occur sequentially at very different solar radii. The inner MSW process would have somewhat different parameters than those for LMA, but the single number from KamLAND is not very restrictive. The outer RSFP process requires that the sterile state have a much smaller mass difference to achieve resonance. If the LSND experiment [18] is correct, at least one light sterile neutrino is required, and it may be more plausible that there be three, possibly having a family symmetry.

If the KamLAND result were not correct, SFP by itself could not explain all the solar data, but RSFP compared with LMA could provide at least as good a global fit [19, 20] to solar data (which depends mainly on the Super-Kamiokande spectrum) and a better fit to average rates of the individual experiments. This is because the neutrino survival probability, while having a resonance pit at a density that suppresses the 0.86 MeV ${}^7\text{Be}$ line (as does the Small-Mixing-Angle (SMA) solution), tends

at high energies toward $1/2$ and hence fits the Super-Kamiokande spectrum, whereas the survival probability goes to unity in the SMA case. The high-energy rise includes the neutral current scattering of the products of the spin-flavor flips, which need to be active, and hence Majorana neutrinos are required in order to fit [20] the SNO data [21]. In the case of subdominant RSFP, the high-energy behavior is determined mainly by the MSW transition, since the observed flux modulation is small ($\sim 10\%$) in the ^8B neutrino region, but the RSFP resonance pit at lower energies could actually improve the overall fit to data.

REVIEW OF PAST EVIDENCE

Whether or not it is the correct interpretation, the RSFP framework provides a convenient way to understand the data, and hence it will be used here, initially to aid in a brief review of the published evidence for solar neutrino flux variability. By analyzing 10^3 simulated data sequences, it was found [3] that the variance of the Homestake solar neutrino data [17] is larger than expected at the 99.9% confidence level (CL). A power spectrum analysis [3] of the data showed a peak at $12.88 \pm 0.02 \text{ y}^{-1}$ (28.4 d), compatible with the rotation rate of the solar radiative zone. Peak widths are computed for a probability drop to 10%. Four sidebands to the 12.88 y^{-1} frequency gave evidence at the 99.8% CL for a latitudinal effect associated with the tilt of the sun's rotation axis, and the latitude dependence was also seen directly in the data at the 98% CL [4].

The GALLEX data [22] showed a peak at $13.59 \pm 0.04 \text{ y}^{-1}$, compatible with the equatorial rotation rate of the deep convection zone. This peak is also in the Homestake data, and a combined analysis of both data sets shows that the 13.59 y^{-1} peak is larger than in either data set alone. Comparison [7] of the power spectrum for the GALLEX data with a probability distribution function for the solar synodic rotation frequency as a function of radius and latitude, derived from SOHO/MDI helioseismology data [23], results in Fig. 1. This map shows that the rotation frequency matches the neutrino modulation in the equatorial section of the convection zone at about 0.8 of the solar radius, R_\odot .

The influence of these rotation frequencies extends even to the corona, since the SXT instrument [24] on the Yohkoh spacecraft provides X-ray evidence for two “rigid” rotation rates, one ($13.55 \pm 0.02 \text{ y}^{-1}$) mainly at the equator, and the other ($12.86 \pm 0.02 \text{ y}^{-1}$) mainly at high latitudes. These values are in remarkable agreement [8] with the neutrino modulation frequencies and also with their equatorial location in one case and non-equatorial in the other; see Fig. 2. A plausible interpretation of this result is that a large-scale magnetic structure deep in the convection zone modulates the neutrino

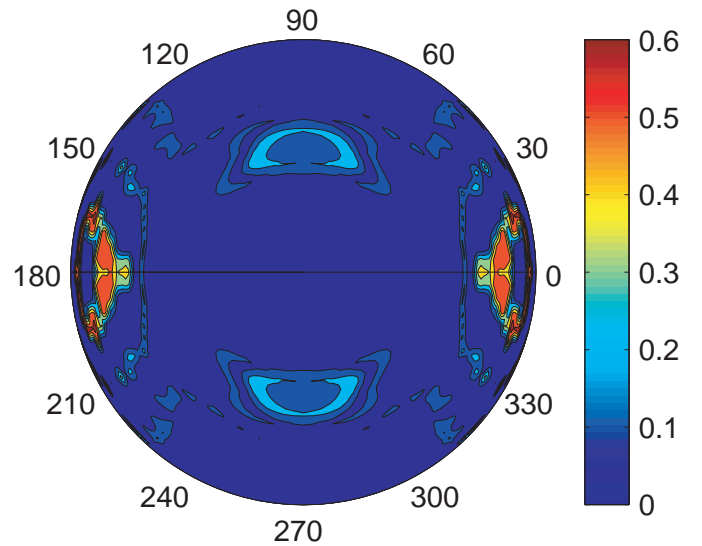


FIG. 1: Map of the resonance statistic of the SOHO/MDI helioseismology and GALLEX data on a meridional section of the solar interior. The only high probability areas (red) are lens-shaped sections near the equator, and all others are low probability.

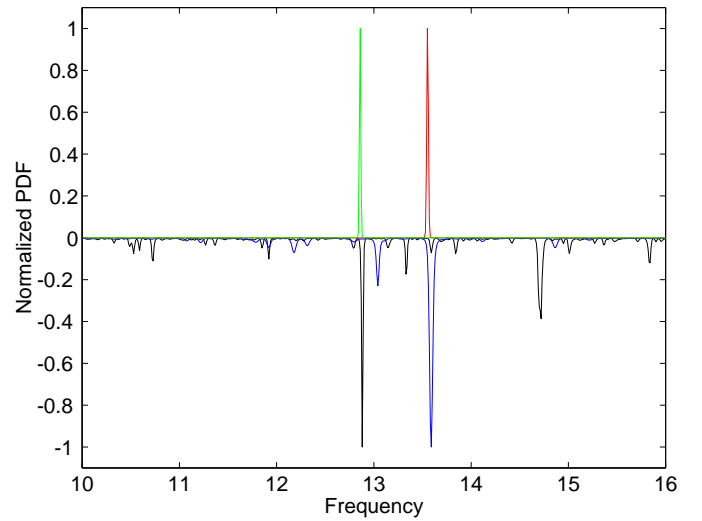


FIG. 2: Comparison of normalized probability distribution functions formed from power spectra of data from SXT equator (red), SXT N60-S60 (green), Homestake (black), and GALLEX (blue). Note that the SXT (red) and GALLEX data are equatorial, and the other two are not. In this and all subsequent figures frequencies are in cycles per year.

flux and is also responsible for the structure of the low- k component of the photospheric magnetic field (where k is wave-number), and that the coronal magnetic field reflects the low- k components rather than the high- k components that arise from granulation.

The fact that coronal X-rays and the neutrino flux both show evidence of two dominant rotation frequen-

cies is quite consistent with similar results of the analyses of other solar variables. For instance, an analysis [25] of the photospheric magnetic field during solar cycle 21 found two dominant magnetic regions: one in the northern hemisphere with synodic rotation frequency $\sim 13.6 \text{ y}^{-1}$, and the other in the southern hemisphere with synodic rotation frequency $\sim 13.0 \text{ y}^{-1}$. Similarly, an analysis [26] of flares during solar cycle 23 found a dominant synodic frequency of $\sim 13.5 \text{ y}^{-1}$ for the northern hemisphere and $\sim 12.9 \text{ y}^{-1}$ for the southern hemisphere. These and other studies show a strong tendency for magnetic structures to rotate either at about 12.9 y^{-1} or at about 13.6 y^{-1} . Since the Sun's magnetic field is believed to originate in a dynamo process at or near the tachocline, it is possible that some magnetic flux is anchored in the radiative zone just below the tachocline, where the synodic rotation frequency is about 12.9 y^{-1} , and some just above the tachocline in the convection zone, where the synodic rotation frequency is about 13.6 y^{-1} . It is also possible that the 12.9 y^{-1} frequency results from a latitudinal wave motion in the convection zone excited by structures at or near the tachocline.

An example of latitudinal oscillatory motion of magnetic structures may be the well-known Rieger-type oscillations (seen in gamma-ray flares, sunspots, etc.) with frequencies of about 2.4, 4.7, and 7.1 y^{-1} [27, 28]. These periodicities may be attributed to r-mode oscillations with spherical harmonic indices $\ell = 3$, $m = 1, 2, 3$, giving frequencies $\nu = 2m\nu_R/\ell(\ell + 1)$, where ν_R is the sidereal rotation rate [$\nu(\text{sid}) = \nu(\text{syn}) + 1$]. These frequencies are also seen in neutrino data [3, 5, 9]. A joint spectrum analysis [9] of Homestake and GALLEX-GNO data yields peaks at 12.88, 2.33, 4.62, and 6.94 y^{-1} , indicating a sidereal rotation frequency $\nu_R = 13.88 \pm 0.03 \text{ y}^{-1}$. While r-mode theory requires $\ell \geq 2$, odd- ℓ values have nonzero poloidal velocity at the equator that could move magnetic regions in or out of the neutrino beam to earth. These r-mode frequencies provide further, and somewhat unexpected, evidence for neutrino flux variations, and we return later to another observation of them.

OBSERVATIONS IN THE NEUTRINO CONTEXT

The difference between the main modulations detected by the Cl and Ga experiments may be explained by the tilt of the solar axis relative to the ecliptic, along with the fact that Cl and Ga neutrinos are produced mainly at quite different radii. The Ga data comes mostly—especially as the fit requires suppressing the ${}^7\text{Be}$ line—from pp neutrinos, which originate predominantly at large solar radius ($\sim 0.2 R_\odot$), so that the wide beam of neutrinos detected on earth is insensitive to axis tilt. Thus the beam of neutrinos detected by the Ga experiments exhibits no seasonal variation and can be modulated by the equatorial structure indicated in Fig. 1,

leading to the observed frequency at about 13.6 y^{-1} . On the other hand, the Homestake experiment detects neutrinos produced from a smaller sphere ($\sim 0.05 R_\odot$), so that the axis tilt causes these neutrinos mainly to miss the equatorial structure of Fig. 1 and instead sample nonzero latitudes where the 12.9 y^{-1} modulation may be more significant. Twice a year axis tilt has no effect for these neutrinos, leading to a seasonal variation in the measured flux [4].

The 13.6 y^{-1} frequency, located as in Fig. 1, represents a modulation of the pp neutrinos which are at or near the steeply falling edge of the neutrino survival probability as it dips toward the RSFP resonance pit. This pit, which suppresses the ${}^7\text{Be}$ neutrinos, is where the largest value of the mass-squared difference between the initial and final states, divided by their energy, satisfies

$$\Delta m^2/E = 2\sqrt{2}G_F N_{\text{eff}}, \quad (1)$$

and is essentially the same as for an MSW resonance [15], since it also arises from a difference in forward-scattering amplitudes of the two states. Ignoring angle factors, for MSW $N_{\text{eff}} = N_e$ (the electron density), and for RSFP and active-active transitions, $N_{\text{eff}} = N_e - N_n$ for Majorana neutrinos, where N_n is the neutron density (about $N_e/6$ in the region of interest in the Sun). For Dirac neutrinos $N_{\text{eff}} = N_e - N_n/2$, but for RSFP alone (not the subdominant case), only Majorana neutrinos fit all the solar data. Using the N_e and N_n values at the $0.8 R_\odot$ location of Fig. 1 in Eq. (1) results in $\Delta m^2/E \sim 10^{-14} \text{ eV}$. This value is that which is required to have the resonance pit suppress ${}^7\text{Be}$ neutrinos and hence fit the solar data. N_{eff} varies exponentially with solar radius and would be quite different for a somewhat changed neutrino modulation frequency. In the RSFP subdominant case, such a location is also needed, but for the SFP case this agreement would be irrelevant, since $\Delta m^2/E$ must be very different.

CHANGES WITH SOLAR CYCLE

It is well known that the convection zone magnetic field changes with the solar cycle, so the neutrino modulation features described above are not permanent. It has been argued [29] that an RSFP effect would have to be in the radiative zone, where the field does not change with the solar cycle, on the assumption that solar cycle variations are not manifested. On the contrary, we show here that solar cycle changes play an important role. Variations in neutrino rates are difficult to observe, since changes in field magnitude would be undetectable if the transition remains adiabatic, and even if flux modulation results, average rates may vary only slightly. The feature that is most sensitive to field magnitude or radial variations is the intersection of the very steeply falling pp neutrino spectrum with the edge of the RSFP resonance pit.

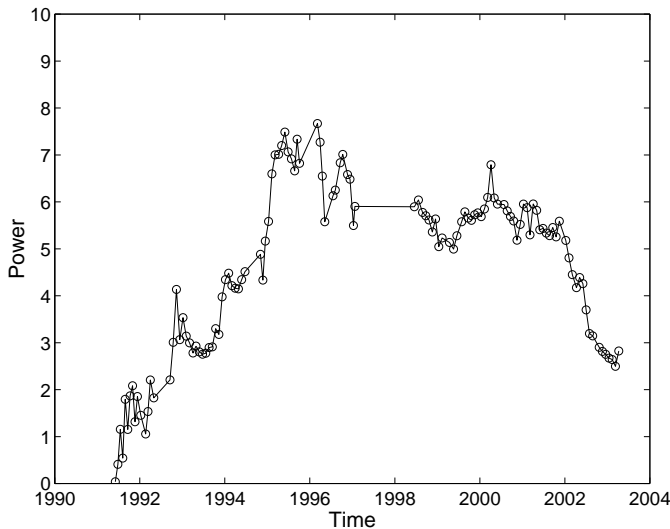


FIG. 3: Running Rayleigh power, as a function of end time, for frequency 13.59 y^{-1} from the GALLEX-GNO data. Note that the power builds up from the start of data taking after the 1990 solar maximum until the 1996.8 solar minimum, after which there is little evidence for that frequency.

The shape of the neutrino transition probability depends not only on the resonance location, Eq. (1), but also on the product of the magnetic moment and magnetic field. Thus a change in field will shift the intersection of the pp spectrum and resonant pit edge and change the degree of modulation. As can be seen in Fig. 3, the 13.6 y^{-1} frequency associated with these neutrinos increased in strength from the start of data taking after the solar maximum of 1989.6 to the solar minimum of 1996.8, after which the modulation becomes weak. Also it was during that cycle that the main buildup in the strength of the 12.9 y^{-1} oscillation was detected by Homestake. The SXT X-ray data, with which these two frequencies had remarkable agreement [8], also came from that same solar cycle.

Another feature attributable to a time variation of the intersection of the pp spectrum with the edge of the RSFP resonance pit is the appearance [6] of a bimodal flux distribution in the Ga data, as shown in Fig. 4. A single peak would be expected if there were no flux modulation. This distribution is clearly evident during the same solar maximum to solar minimum period when the flux is binned appropriately using individual runs, instead of averaged over several data runs. This neutrino flux effect also diminishes after the solar minimum. Adding to the significance of this result is the plot of Fig. 5, which shows that when the end times of runs are reordered according to the phase of the 13.59 y^{-1} rotation, the flux values are low in one-half of the cycle and high in the other.

It is unfortunate that the Homestake experiment, which detected mainly the ^8B neutrinos (the only neutrino component registered by Super-Kamiokande)

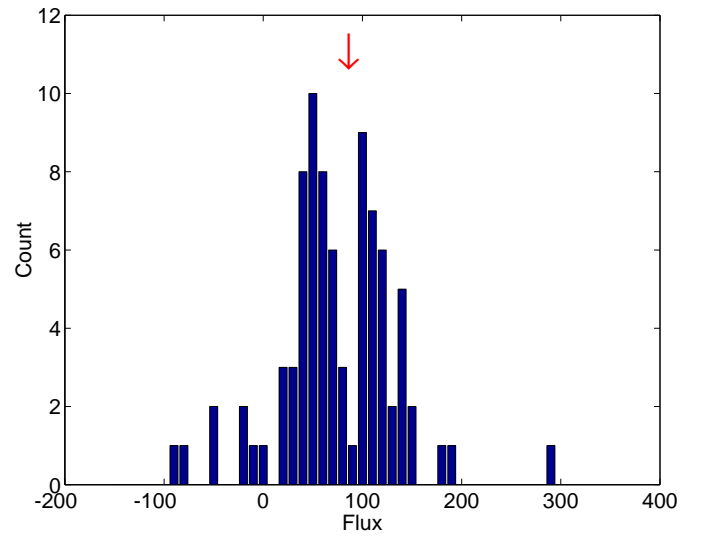


FIG. 4: Histogram of GALLEX data. The arrow indicates the maximum-likelihood estimate of the flux (in SNU).

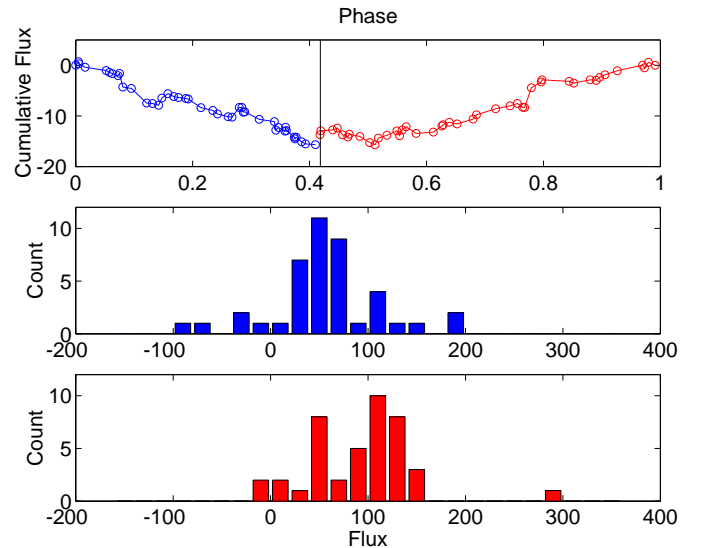


FIG. 5: Normalized GALLEX flux (in SNU) measurement runs (prior to 1997) reordered according to the phase of the 13.59 y^{-1} solar modulation. The division in phase is made so as to have equal numbers of events in the descending (blue) and ascending (red) parts of the cycle.

ceased operation before Super-Kamiokande started. As a result, there is no way to predict from other solar neutrino experiments what neutrino flux variation should have been detected by Super-Kamiokande during its operation from May 1996 (near solar minimum) until July 2001 (near solar maximum). However, it is possible to compare Super-Kamiokande measurements with other solar variables that reflect the influence of the Sun's internal magnetic field.

SUPER-KAMIOKANDE DATA ANALYSIS

Recently the Super-Kamiokande group released [12] flux measurements in 184 bins of about 10 days each. The flux measurements vary over the range 2 : 1, and the fractional error of the measurement (averaged over all bins) is 0.14. Because of the regularity of the binning, the “window spectrum” (the power spectrum of the acquisition times) has a huge peak (power $S > 120$) at a frequency of $\nu = 35.98 \text{ y}^{-1}$ (period 10.15 d). (Note that the probability of obtaining a power of strength S or more by chance at a specified frequency is [30] e^{-S} .) This regularity in binning inevitably leads to severe aliasing of the power spectrum of the flux measurements, producing consequences explored below.

Analysis of the data in 10-day bins by a likelihood procedure outlined in the Appendix, in which the start and stop times for each bin were used so as to take into account the time over which data were taken, gave [13] the strongest peak in the range 0 to 100 y^{-1} at $\nu = 26.57 \text{ y}^{-1}$ with $S = 11.26$, and the next strongest peak at $\nu = 9.42 \text{ y}^{-1}$ with $S = 7.29$. Milsztajn, and subsequently the Super-Kamiokande group, used the Lomb-Scargle analysis method [30], which assigns data acquisition to discrete times (in this case chosen to be the mid-time of each bin) rather than to extended intervals. This “delta-function” form for the time window function is inappropriate, since the length of each bin is comparable with the periods of some of the oscillations of interest. It is also significant that the likelihood method takes measurement errors into account, whereas the Lomb-Scargle method as they used it does not. The Lomb-Scargle analysis by the Super-Kamiokande group gave [13] $S = 10.7$ at $\nu = 26.55 \text{ y}^{-1}$, which was stated to correspond to 98.6% CL, while the ignored peak at 9.41 y^{-1} had $S = 6.3$. Subsequently, the Super-Kamiokande group modified their analysis to take account of the non-uniformity of data collection, assigning the flux and error measurements for each bin to a “mean live time” rather than the mid-time. This has resulted in a reduction to $S = 7.51$ of the power at 26.55 y^{-1} , but an increase to 6.67 in the power of the peak at 9.41 y^{-1} .

We have recently modified our likelihood analysis to take account of the non-uniformity in data acquisition, dividing each bin into two parts (before and after the mean live time) with appropriate weightings. In contrast to the sensitivity of the Lomb-Scargle procedure to non-uniformity in the data acquisition process, we find the likelihood procedure to be quite insensitive to the non-uniformity represented by the Super-Kamiokande data. The “single boxcar” and “double boxcar” time window functions yield essentially the same power spectrum, that shown in Figure 6, in which the peaks at 26.55 y^{-1} and at 9.42 y^{-1} still have $S = 11.26$ and 7.29, respectively. This again shows the superiority of the likelihood method over

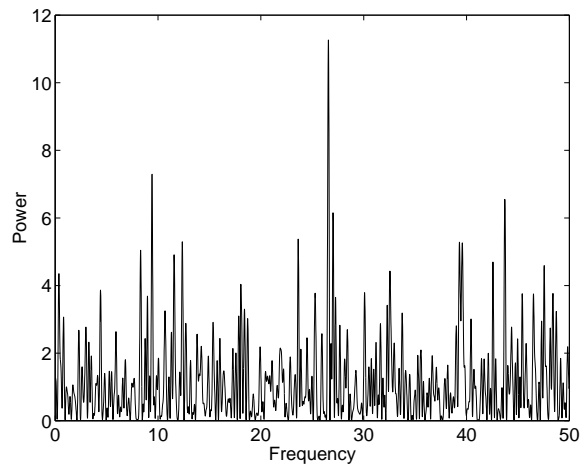


FIG. 6: Power Spectrum of Super-Kamiokande 10-day data computed by the likelihood method.

the Lomb procedure used, since the latter employed only the mean time, whereas the former utilized mean, start, and stop times, and more importantly, the measurement errors.

We previously noted [13] that 9.41 y^{-1} and 26.57 y^{-1} sum to 35.98 y^{-1} , which is the sampling frequency, from which we inferred that one peak is spurious, being an alias of the other. Since the peak at 26.57 y^{-1} had the bigger power, and since it falls in the band of twice the synodic rotation frequency, we assumed that the peak at 9.41 y^{-1} was merely an alias. However, when the Super-Kamiokande data were subdivided into 5-day bins [14], the peak at 26.57 y^{-1} disappeared, but the peak at 9.41 y^{-1} remained. Hence it is now clear that the peak at 26.57 y^{-1} was an alias of the peak at 9.41 y^{-1} , not the other way around.

We have recently analyzed the new Super-Kamiokande 5-day data using the likelihood procedure, taking account of the experimental error estimates, the mean live time and the start and end time of each bin [31]. The resulting power spectrum is shown in Figure 7. The biggest peak, A, in the range 0– 100 y^{-1} is that at $9.43 \pm 0.05 \text{ y}^{-1}$, which now has the enhanced power $S = 11.51$. In agreement with the analysis of the Super-Kamiokande group, we find that the peak at 26.57 y^{-1} has disappeared. Hence 9.43 y^{-1} is the primary peak, and the 26.57 y^{-1} peak was an alias in the 10-day data. Since the 5-day binning is also very regular, the power spectrum of the timing now has a huge peak at 72.01 y^{-1} (period 5.07 days), so an alias peak would be expected at $72.01 - 9.43 = 62.58 \text{ y}^{-1}$, and we do indeed find a peak (not shown in Fig. 7) at $\nu = 62.56 \pm 0.08 \text{ y}^{-1}$ with $S = 5.36$. There are also notable peaks at $39.28 \pm 0.05 \text{ y}^{-1}$ ($S = 8.91$), labeled C, and $43.72 \pm 0.06 \text{ y}^{-1}$ ($S = 9.83$), designated B in Fig. 7. The latter two peaks, plus that at 9.43 y^{-1} are the three strongest peaks in the range 0– 100 y^{-1} . The 39 y^{-1} and 44 y^{-1} peaks are much weaker in the 10-day

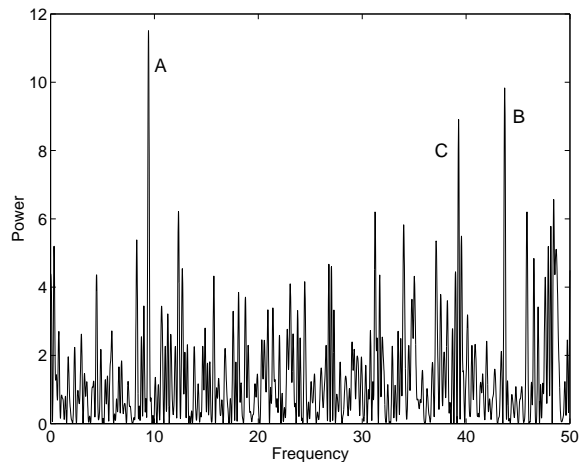


FIG. 7: Power Spectrum of Super-Kamiokande 5-day data computed by the likelihood method, taking account of measurement error, start time, and end time, of each bin.

data, presumably because the sampling time is too long.

EXPLANATION FOR THE PEAK FREQUENCIES

To understand these three peaks, it is helpful to seek guidance from measurements of the solar magnetic field. A power spectrum out to 120 y^{-1} of the photospheric field at Sun-center during the Super-Kamiokande data-acquisition interval is shown in Figure 8. We see that the fundamental and second harmonic of the rotation frequency are virtually absent, but there is a remarkable sequence of higher harmonics. By forming the combined spectrum statistic [9] of the third through the seventh harmonics, we obtain the estimate $13.20 \pm 0.14 \text{ y}^{-1}$ for the synodic rotation frequency of the photospheric magnetic field, leading to the value $14.20 \pm 0.14 \text{ y}^{-1}$ for the sidereal rotation frequency.

We see that peak C, at 39.28 y^{-1} , falls within the band of frequencies, $39.60 \pm 0.42 \text{ y}^{-1}$, of the third harmonic of the synodic rotation frequency of the magnetic field. We have applied the shuffle test [3, 32], randomly re-assigning flux and error measurements (kept together) to time bins. For this purpose, the shuffle test is more reliable than Monte Carlo simulations, since actual data are used. In this way we find that only 5 of 1,000 simulations yield a power larger than 8.91 (the power of peak C) in this search band. It appears, therefore, that peak C may be attributed to the effect of the Sun's internal inhomogeneous magnetic field that necessarily rotates with the ambient medium. To check this assumption, we have determined the frequency for which the neutrino and magnetic data show the strongest correlation by means of the joint spectrum statistic [9]. This frequency is found to be 39.56 y^{-1} . Figure 9 shows the cumulative Rayleigh powers derived from the neutrino and magnetic data for

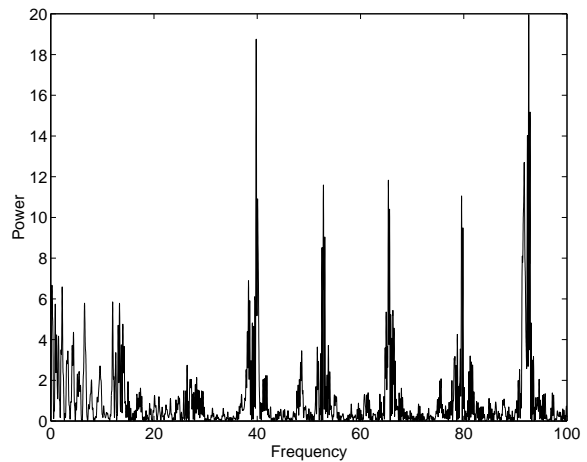


FIG. 8: Power spectrum of the disk-center solar magnetic field for the interval of operation of Super-Kamiokande.

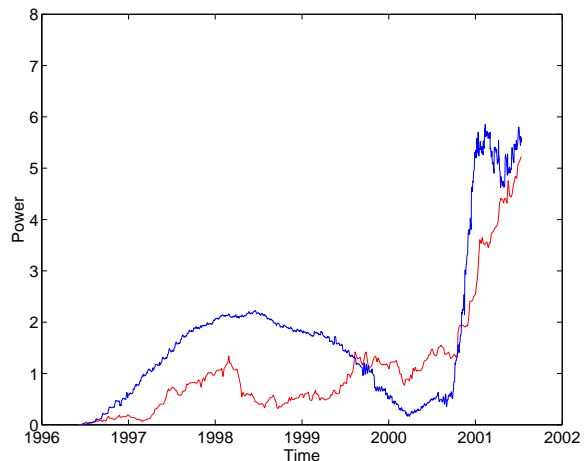


FIG. 9: Cumulative contribution to the final Rayleigh power of disk-center magnetic field (blue) and 5-day Super-Kamiokande data (red) for frequency 39.56 y^{-1} . The steep rise begins near solar maximum (2000.6).

this frequency. We see that there is a remarkable correspondence, both powers growing from 1996 until 1998, then decreasing until about 2000.6 (solar maximum), after which both increase sharply, indicating again the influence of the solar cycle variations of magnetic structures in the convection zone.

We now consider peak A at 9.43 with power 11.51, and peak B at 43.72 with power 9.83. We presented evidence above for r-mode oscillations [28] in the Homestake and GALLEX-GNO data that appear to be the origin of the well-known Rieger oscillation [27] and of similar “Rieger-type” oscillations [33] that have been discovered in recent years. We therefore examine the possibility that peaks A and B may be related to such oscillations interpreted as r modes.

R-modes are retrograde waves that, in a uniform and

uniformly rotating sphere, have frequencies

$$\nu(\ell, m, \text{syn}) = m(\nu_R - 1) - \frac{2m\nu_R}{\ell(\ell + 1)} \quad (2)$$

as seen from Earth, where ℓ and m are two of the usual spherical-harmonic indices, and ν_R is the sidereal rotation frequency (in cycles per year). If r-mode oscillations are to influence the solar neutrino flux, they must interfere with magnetic regions that co-rotate with the ambient medium. The interference frequencies will be given by

$$\nu = \left| m(\nu_R - 1) - \frac{2m\nu_R}{\ell(\ell + 1)} \pm m'(\nu_R - 1) \right| \quad (3)$$

where m' , the azimuthal index for the magnetic structure, may be different from that of the r-mode. For $m' = m$, equation (3) yields the frequency

$$\nu(\ell, m, \text{rot}) = \frac{2m\nu_R}{\ell(\ell + 1)}, \quad (4)$$

for the minus sign, and

$$\nu(\ell, m, \text{alias}) = 2m(\nu_R - 1) - \frac{2m\nu_R}{\ell(\ell + 1)} \quad (5)$$

for the plus sign. The frequencies given by (4) are the well-known Rieger-type frequencies. We may regard the frequencies given by (5) as aliases of these frequencies.

For $\ell = 2$ and $m = 2$ and for the range of values of ν_R inferred from the magnetic-field data, equation (4) leads us to expect oscillations in the band 9.47 ± 0.09 , and equation (5) leads us to expect oscillations in the band 43.33 ± 0.47 . We see that the peaks A and B fall within these bands. On applying the shuffle test, we find only 2 cases out of 10,000 in which a peak with power larger than 11.51 occurs in the band 9.47 ± 0.09 , and only 3 cases out of 1,000 that yield a power larger than 9.83 in the band 43.33 ± 0.47 . Figure 10 shows the cumulative Rayleigh powers at these two frequencies as a function of time. These two frequencies not only have a very similar trend in their time evolution, but also some of the fine structure is even similar, indicating that they both originate in the same internal oscillation, an r-mode with $\ell = 2, m = 2$. Note the contrast between Figs. 9 and 10, showing the different origins of the A and B peaks from that of C.

PREDICTIONS AND CONCLUSIONS

While in the future an especially good test of these ideas will come from real-time data taken at low enough energies to see the effect of the pp neutrino spectrum, a very interesting check should occur soon from SNO data. There has been a promise to use one-day bins, so the

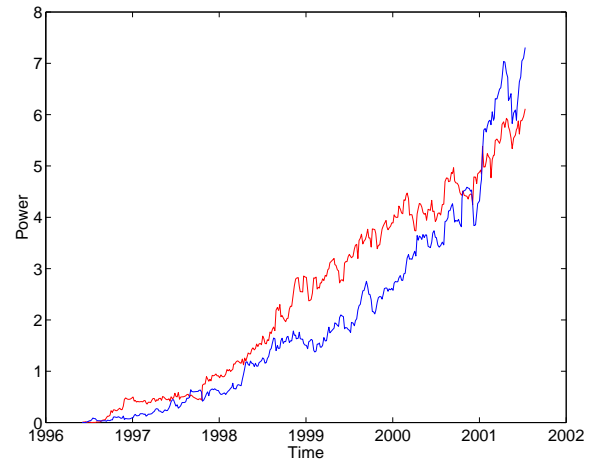


FIG. 10: Cumulative contribution to the final Rayleigh powers of oscillations at 9.42 y^{-1} (red) and 43.72 y^{-1} (blue).

alias peak at 62.56 y^{-1} should not be seen. Figure 9 indicates that the 39.3 y^{-1} peak should be present, and with that shorter sampling time some of the higher harmonics of the magnetic field rotation may be observed also. Figure 10 indicates that the Rieger-type frequencies may also be present. Especially interesting could be a comparison of the amplitudes of the flux modulations for the charged-current and neutral-current interactions, since with spin change as well as flavor change responsible, in principle a difference in these two could indicate that the neutrinos are Majorana particles. If, however, the transitions are all to the sterile state, then the result could not distinguish Majorana from Dirac neutrinos.

The analysis of Super-Kamiokande data, when combined with the results of analyses of Cl and Ga data, yields a variety of evidence for variability of the solar neutrino flux. Since the KamLAND experiment supports the LMA solution, flux variability can be accommodated by adding SFP or RSFP as a subdominant process. Either of these spin-flip processes in a subdominant role requires at least one light sterile neutrino, and RSFP appears favored by the flux data. Thus, a definitive result on neutrino flux time dependence, which can best be carried out using a combined analysis of all experiments, could lead to important new physics involving large transition magnetic moments and sterile neutrinos.

ACKNOWLEDGMENTS

We are indebted to many friends for assistance and helpful discussions. D.O.C. is supported by a grant from the Department of Energy No. DE-FG03-91ER40618, and P.A.S. is supported by grant No. AST-0097128 from the National Science Foundation.

APPENDIX: BRIEF EXPLANATION OF THE LIKELIHOOD CALCULATION

The log-likelihood that the data x_r may be fit by a given functional form X_r is given [31] by

$$L = -\frac{1}{2} \sum_{r=1}^R \frac{(x_r - X_r)^2}{\sigma_r^2}, \quad (1)$$

apart from a constant term, where $r = 1, \dots, R$ enumerates the data bins. We adopt

$$x_r = \frac{g_r}{\text{mean}(g_r)} - 1, \quad (2)$$

where g_r are the flux measurements, and scale the error estimates accordingly. We adopt the functional form

$$X_r = \frac{1}{D_r} \int_{t_{gr}}^{t_{er}} dt (A e^{i2\pi\nu t} + A^* e^{-i2\pi\nu t}), \quad (3)$$

where D_r is the duration of each bin. Then, for each frequency, we adjust the amplitude A to maximize the likelihood [3].

What is significant is not the actual log-likelihood as computed from (1), but the increase in the log-likelihood over the value that corresponds to a constant flux, which is given (apart from the same constant term) by

$$L_0 = -\frac{1}{2} \sum_{r=1}^R \frac{x_r^2}{\sigma_r^2}. \quad (4)$$

Hence the relative log-likelihood, which is equivalent to the power spectrum, is given by

$$S = L - L_0, \quad (5)$$

i.e., by

$$S = \frac{1}{2} \sum_{r=1}^R \frac{x_r^2}{\sigma_r^2} - \frac{1}{2} \sum_{r=1}^R \frac{(x_r - X_r)^2}{\sigma_r^2}. \quad (6)$$

Application of the formalism above to one frequency in the Super-Kamiokande data shows the magnitude of the flux modulation. For $\nu = 9.43$, and for zero time chosen arbitrarily to be the date 1970.00, we find that $A = 0.0192 - 0.0291i$. This corresponds to a depth of modulation of the neutrino flux of 7%.

-
- [1] K. Eguchi et al., *Phys. Rev. Lett.* **90**, 021802 (2003).
 [2] C.-S. Lim and W.J. Marciano, *Phys. Rev. D* **37**, 1368 (1988); E.Kh. Akhmedov, *Sov. J. Nucl. Phys.* **48**, 382 (1988) and *Phys. Lett.* **B213**, 64 (1988).
 [3] P.A. Sturrock, G. Walther and M.S. Wheatland, *Astrophys. J.* **491**, 409 (1997).

- [4] P.A. Sturrock, G. Walther and M.S. Wheatland, *Astrophys. J.* **507**, 978 (1998).
 [5] P.A. Sturrock, J.D. Scargle, G. Walther and M.S. Wheatland, *Astrophys. J.* **523**, L177 (1999).
 [6] P.A. Sturrock and J.D. Scargle, *Astrophys. J.* **550**, L101 (2000).
 [7] P.A. Sturrock and M.A. Weber, *Astrophys. J.* **565**, 1366 (2002).
 [8] P.A. Sturrock and M.A. Weber, “Multi-Wavelength Observations of Coronal Structure and Dynamics—Yohkoh 10th Anniversary Meeting” (COSPAR Colloquia Series, P.C.H. Martens and D. Cauffman, eds., 2002), p. 323.
 [9] P.A. Sturrock, astro-ph/0304148; hep-ph/0304106; P.A. Sturrock and M.S. Wheatland, astro-ph/0307353.
 [10] E.Kh. Akhmedov and J. Pulido, *Phys. Lett.* **B553**, 7 (2003). This work does not provide for sufficient flux modulation with new limits on solar antineutrinos. Instead, J. Pulido is investigating SFP with a sterile neutrino, and we are grateful to him for very helpful discussions.
 [11] S. Fukuda et al., *Phys. Rev. Lett.* **86**, 5651 (2001).
 [12] M.B. Smy, hep-ex/0206016 and <http://www-sk.icrr.u-tokyo.ac.jp/sk/lowe/index.html>
 [13] P.A. Sturrock and D.O. Caldwell, *Bull. Am. Astron. Soc.* **34**, 1314 (2002); P.A. Sturrock, hep-ph/0304073, *Astrophys. J.* (in press). D.O. Caldwell and P.A. Sturrock, hep-ph/0305303; A. Milsztajn, hep-ph/0301252; M. Nakahata, <http://www-sk.icrr.u-tokyo.ac.jp/sk/lowe/frequencyanalysis/index.html>
 [14] J. Yoo et al., hep-ex/0307070.
 [15] L. Wolfenstein, *Phys. Rev. D* **17**, 2369 (1978); *Phys. Rev. D* **20**, 2634 (1979); S.P. Mikheyev and A.Yu. Smirnov, *Sov. J. Nucl. Phys.* **42**, 913 (1985); *Nuovo Cimento* **9C**, 17 (1986).
 [16] P.C. de Holanda and A.Yu. Smirnov, hep-ph/0307266.
 [17] B.T. Cleveland et al., *Astrophys. J.* **496**, 505 (1998).
 [18] A. Aguilar et al., *Phys. Rev. D* **64**, 112007 (2001) and earlier references therein.
 [19] M.M. Guzzo and H. Nunokawa, *Astropart. Phys.* **12**, 87 (1999); J. Pulido and E.Kh. Akhmedov, *Astropart. Phys.* **13**, 227 (2000); E.Kh. Akhmedov and J. Pulido, *Phys. Lett.* **B485**, 178 (2000); O.G. Miranda, C. Peña-Garay, T.I. Rashba, V.B. Semikoz and J.W.F. Valle, *Nucl. Phys.* **B595**, 360 (2001) and *Phys. Lett.* **B521**, 299 (2001); J. Pulido, *Astropart. Phys.* **18**, 173 (2002).
 [20] B.C. Chauhan and J. Pulido, *Phys. Rev. D* **66**, 053006 (2002) includes the SNO data in the fits.
 [21] Q.R. Ahmad et al., *Phys. Rev. Lett.* **89**, 011301 and 011302 (2002).
 [22] W. Hampel et al., *Phys. Lett.* **B447**, 127 (1999); M. Altmann et al., *Phys. Lett.* **B490**, 16 (2000).
 [23] J. Schou et al., *Astrophys. J.* **505**, 390 (1998).
 [24] S. Tsuneta et al., *Solar Phys.* **136**, 37 (1991).
 [25] E. Antonucci et al., *Astrophys. J.* **360**, 296 (1998).
 [26] T. Bai, *Bull. Am. Astron. Soc.* **34**, 953 (2002).
 [27] E. Rieger et al., *Nature* **312**, 623 (1984).
 [28] J. Papaloizou, and J.E. Pringle, *Mon. Not. R. Astron. Soc.* **182**, 423 (1978); J. Provost, G. Berthomieu, and A. Rocca, *Astron. Astrophys.* **94**, 126 (1981); H. Saio, *Astrophys. J.* **256**, 717 (1982).
 [29] A. Friedland and A. Gruzinov, *Astropart. Phys.* **19**, 575 (2003).
 [30] N. Lomb, *Astrophys. Space Sci.* **39**, 447 (1996); further developed by J.D. Scargle, *Astrophys. J.* **263**, 835

- (1982); *Astrophys. J.* **343**, 874 (1989).
- [31] P.A. Sturrock, *Astrophys. J.* **594**, 1102 (2003).
- [32] J.N. Bahcall and W.H. Press, *Astrophys. J.* **370**, 730 (1991).
- [33] T. Bai, *Astrophys. J.* **388**, L69 (1992); *Solar Phys.* **150**, 385 (1994); J.N. Kile, and E.W. Cliver, *Astrophys. J.* **370**, 442 (1991).